LUND UNIVERSITY

Generation of trisomies in cancer cells by multipolar mitosis and incomplete cytokinesis.

Gisselsson Nord, David; Jin, Yuesheng; Lindgren, David; Persson, Johan; Gisselsson, Lennart; Hanks, Sandra; Sehic, Daniel; Holmquist Mengelbier, Linda; Øra, Ingrid; Rahman, Nazneen; Mertens, Fredrik; Mitelman, Felix; Mandahl, Nils

Link to publication

LUND UNIVERSITY

PO Box 117
221 00 Lund
+46 46-222 00 00

Biological Sciences: Medical Sciences

Generation of trisomies in cancer cells by multipolar mitosis and incomplete cytokinesis

David Gisselsson[a,b,1], Yuesheng Jin[a], David Lindgren[c], Johan Persson[d], Lennart Gisselsson[d], Sandra Hanks[e], Daniel Sehic[a], Linda Holmquist Mengelbier[a], Ingrid Øra[f], Nazneen Rahman[e], Fredrik Mertens[a], Felix Mitelman[a], Nils Mandahl[a]

[a]Department of Clinical Genetics, Lund University, University and Regional Laboratories, University Hospital, SE-221 85 Lund, Sweden; [b]Department of Pathology, University and Regional Laboratories, University Hospital, SE-221 85 Lund, Sweden; [c]Department of Laboratory Medicine, Center for Molecular Pathology, Lund University, SE-205 02 Malmö, Sweden; [d]Phase Holographic Imaging AB, Lund Bioinkubator, BioMedical Center D10, SE-221 84 Lund, Sweden; [e]Section of Cancer Genetics, Institute of Cancer Research and Royal Marsden Hospital, Sutton, Surrey, SM2 5NG, UK; and the [f]Department of Paediatric Oncology and Haematology, University Hospital, SE-221 85 Lund, Sweden

Key words: trisomy, spindle assembly checkpoint, cancer, multipolar mitosis, cytokinesis

[1]To whom correspondence may be addressed. David Gisselsson. Department of Clinical Genetics, University Hospital, SE-221 85 Lund, Sweden. Phone: +46 46 173418. Fax: +46 46 131061. E-mail: david.gisselsson_nord@med.lu.se

Abstract

One extra chromosome copy (trisomy) is the most common type of chromosome aberration in cancer cells. The mechanisms behind the generation of trisomies in tumor cells are largely unknown, although it has been suggested that dysfunction of the spindle assembly checkpoint (SAC) leads to an accumulation of trisomies through failure to correctly segregate sister chromatids in successive cell divisions. Using Wilms tumor as a model for cancers with trisomies, we now show that trisomic cells can form even in the presence of a functional SAC through tripolar cell divisions in which sister chromatid separation proceeds in a regular fashion while cytokinesis failure nevertheless leads to an asymmetrical segregation of chromosomes into two daughter cells. A model for the generation of trisomies by such asymmetrical cell division accurately predicted several features of clones having extra chromosomes *in vivo*, including the ratio between trisomies and tetrasomies and the observation that different trisomies found in the same tumor occupy identical proportions of cells and co-localize in tumor tissue. Our findings provide the first experimentally validated model explaining how multiple trisomies can occur in tumor cells that still maintain accurate sister chromatid separation at metaphase-anaphase transition and thereby physiologically satisfy the SAC.

\body

Introduction

Whole chromosome gains (typically trisomies and tetrasomies) are the most common type of chromosome aberration in cancer cells (Mitelman Database of Chromosome Aberrations in Cancer 2010, http://cgap.nci.nih.gov/Chromosomes/Mitelman). It is well established that chromosomal alterations in cancer can arise as a consequence of abnormal segregation of chromosomes at mitosis, but it remains to be shown precisely how extra copies of whole chromosomes are gained. It has been suggested that deficiency of the spindle assembly checkpoint (SAC) or other key mechanisms controlling sister chromatid separation could promote the generation of trisomies in cancer cells through a continuously elevated rate of concurrent chromosome gain and loss (non-disjunction) at metaphase-anaphase transition (1-4). The SAC deficiency model has been challenged by the fact that mutations in mitotic checkpoint genes have been found only in a minority of human cancers (3-7), but the absence of such mutations could still be explained by epigenetic modifications of mitotic control genes or by mutations in SAC genes that are not yet characterized. Therefore, it has remained difficult to experimentally validate the association between SAC deficiency and trisomies. This problem could be circumvented by estimating directly the rate of sister chromatid separation failure at mitosis. To do this, we used fluorescence *in situ* hybridization (FISH) to monitor the segregation of individual chromosomes in ana-telophase cells. This method was then applied to Wilms tumor (WT) -- a prototypical model for cancers with whole chromosome gains, showing polysomies in the majority of cases with abnormal karyotypes, of which 62% have two or more co-existing trisomies and 16% have tetrasomies (Mitelman Database of Chromosome Aberrations in Cancer 2010). In contrast to previous assumptions, we find that continuous generation of trisomies through SAC deficiency is unlikely to explain the generation of multiple whole chromosomes

3

gains in these tumors. Instead, our data indicate that a previously uncharacterized mechanism consisting of combined spindle multipolarity and cytokinesis failure could explain trisomy generation in WT.

Results

First we determined the base-line rate of chromosome missegregation in short-term cultures from normal dermal fibroblast samples (Table S1) and found that the median rate was 4.0×10^{-4} (range $3.3-4.1 \times 10^{-4}$) per chromosome per mitosis, equivalent to one missegregation in approximately 50 cell divisions (Fig. 1A and B; Fig. S1A). As a positive control for SAC deficiency, we then used cells from patients with mosaic variegated aneuploidy (MVA) syndrome, a rare autosomal recessive condition associated with a high rate of constitutional mosaic aneuploidies, predominantly trisomies and monosomies. A sub-group of MVA patients exhibit bi-allelic mutations of the SAC key gene *BUB1B* (8). We analyzed fibroblasts from three MVA cases, all of which showed SAC deficiency by failure to arrest normally at metaphase during nocodazole exposure; two with and one without biallelic *BUB1B* mutations (8). All three MVA cases exhibited rates of chromosome missegregation that were more than ten-fold higher compared to normal fibroblasts (Table S1; Fig. 1C). Ana-telophase cells in which missegregation was detected showed a bipolar orientation and had only two centrosomes, as shown by combined FISH and immunofluorescence in one of the MVA cases (Fig. S1B). Elevated rates of missegregation in bipolar mitoses were also found in the colorectal carcinoma cell lines SW480 and LoVo, known to exhibit SAC deficiency (1). In contrast, the rate of missegregation in bipolar mitoses was similar to fibroblasts in the SAC-competent colorectal cancer cell line DLD1. Notably, all three colorectal cancer cell lines also showed multipolar ana-telophase cells co-ordinated by multiple centrosomes. None of these cell divisions produced daughter cells with the same chromosome

copy number as that of the mother cell, resulting in a high missegregation frequency. Thus, SW480 and LoVo exhibited at least two types of chromosomal instability, one caused by SAC dysfunction and one by centrosomal disturbances, consistent with previous studies (1, 9).

We then screened cells from five primary WTs and the WiT49 WT cell line, all of which had hyperdiploid-triploid karyotypes with whole chromosome gains, typically trisomies. Even though aneuploid cells were specifically selected for analysis, to avoid scoring contaminating non-neoplastic cells in primary tumors, a significantly elevated rate of missegregation compared to normal fibroblasts was not observed in bipolar ana-telophase configurations in WT cells (P=0.39; Mann-Whitney U test). WTs exhibited rates of missegregation at bipolar mitosis that were on average elevenfold lower than those of SAC deficient MVA fibroblasts and colorectal cancer cell lines (P=0.0078). However, all six WTs showed ana-telophase cells in multipolar configurations (0.8-4.2% of anaphase cells, compared to none in >1500 fibroblasts scored; Fig. S1C). These cell divisions resulted in unequal copy numbers in sister nuclei at rates that were 16-128 times higher than those resulting from missegregation at bipolar mitosis.

Multipolar cell divisions have been observed in many human tumor types but their role in tumorigenesis has remained disputed, primarily because clonogenic survival of daughter cells from such mitoses appears to be significantly reduced (10, 11). To assess whether the observed multipolar cell divisions might still contribute to clonal evolution in WT, we performed holographic time lapse imaging of WiT49 cells. By using a low-intensity laser to provide enhanced contrast imaging, this method allows periods of continuous observations of growing cells for more than one week without the need of transfection with fluorescent markers, which might otherwise induce alterations in cellular phenotype. Because >80% of the multipolar anaphase cells observed in the primary tumors were tripolar, we analysed only multipolar mitoses that divided towards three anaphase poles. Surprisingly, only a minority (2/18) of these divisions

5

resulted in three daughter cells (Fig. 1D, S2A, and S2B). The majority resulted either in multinucleate single daughter cells (7/18) or, more commonly (9/18), underwent cytokinesis with complete ingression of the cleavage furrow along one plane only, while another furrow was typically initiated but failed to show complete ingression (Fig. S2C). Because chromosomes nevertheless segregated towards three poles, the latter mitoses resulted in the formation of two daughter cells, one binucleated and one mononucleated. Of the 18 daughter cells resulting from cytokinesis along only one cleavage plane, three of the binucleated cells during the period of observation again underwent mitosis, in which they showed an intermingling of prometaphase chromosomes, giving rise to a single mitotic plate before cell division (Video S1), demonstrating that cells having undergone this type of cell division may proliferate further. Immunofluorescence on fixed WiT49 cells corroborated that approximately 50% of the tripolar telophase configurations exhibited cleavage along one plane only, as evidenced by a single midbody by beta tubulin staining (Fig. 1E). Furthermore, 66% of cell divisions of this type showed a complete absence of kinetochore MAD2L1 staining, indicating that metaphase-anaphase transition had occurred through satisfaction of the SAC (Fig. 1E, 1F, and S1F). Accordingly, immunofluorescence combined with FISH showed a segregation pattern consistent with amphitelic sister chromatid separation in >80% such ana-telophase configurations in WiT49, including the formation of trisomies in the binucleated daughter cells (Fig. S1D and S1E).

WTs originate from embryonic renal progenitor cells that have undergone maturation arrest (12). To validate our findings in an independent system, we therefore turned to a human embryonic kidney cell line (HEK293D) that was obtained by transforming primary human embryonic kidney cells with sheared human adenovirus type 5 (13), leading to deregulation of the centrosome cycle and multipolar mitoses (14). These cells had acquired copy number alterations for some chromosomes, but many were still retained as disomies in the stem line (15). To

evaluate further whether trisomies could be acquired also in these cells through tripolar mitosis and incomplete cytokinesis, we performed transfection with an *H2B-GFP* construct, allowing concurrent phase contrast and fluorescent imaging in which chromatin and cytokinesis could be studied in real time. Of bipolar HEK293D cell divisions, the vast majority (95%) underwent complete cytokinesis, resulting in two daughter cells (Fig. S3A and S4A; Video S2). In contrast, the majority (80%) of tripolar anaphase configurations showed failure of cytokinesis, typically resulting in one binucleated and one mononucleated daughter cell (Fig. S3B and S4B; Videos S3 and S4); only a minority (20%) underwent complete cytokinesis (Fig. S3C; Video S5). Combined beta tubulin immunofluorescence and FISH for centromeres of chromosomes 3, 4, 7, 9, 11, and 15 (disomic in the HEK293D *H2B-GFP* stem line) was then performed on telo-interphase cells with single cleavage planes and a 2-1 nuclear distribution. Of these, the majority exhibited unbalanced segregation between the two daughter cells, typically with a 3-1 chromosome distribution, resulting in a trisomy in the binucleated daughter cell (Fig. 1G-I, S4C and S4D). Thus, trisomic cells formed through tripolar division coupled to incomplete cytokinesis also in the HEK293D model system, corroborating the data from WiT49.

A diploid cell undergoing tripolar nuclear division with amphitelic sister chromatid separation followed by cytokinesis along only one furrow will result in one hyperdiploid and one hypodiploid daughter cell, with a difference in chromosome number determined by the number of chromosomes present on the metaphase axis along which the cleavage furrow fails to undergo complete ingression (Fig. 2A). Presence of several chromosomes on this axis will result in the simultaneous generation of multiple trisomies and/or tetrasomies in the hyperdiploid daughter cell. This type of cell division is therefore an attractive model for the generation of several whole chromosome gains through a single event. However, the frequency of missegregation in bipolar cell divisions was >0 in WT cells (Table S1) and the possibility that multiple trisomies and/or

7

tetrasomies were generated by sequential gain of chromosomes (Fig. 2B) could therefore not be completely excluded. To test which of the two alternatives that best predicted the pattern of whole chromosome gains in published karyotypes from primary WTs, we analyzed the frequency of tetrasomies in 152 cases having 2 or more whole chromosome gains (Mitelman Database of Chromosome Aberrations in Cancer 2010). The sequential model predicts the highest probability for the acquisition of tetrasomies, as chromosomes already in a trisomic state would have a higher probability than disomic chromosomes for being involved in any subsequent missegregation (Fig. 2C). The tetrasomy frequencies found in the 152 WTs were clearly distinct from those expected from the sequential generation model (Fig. 2B), while they closely mirrored the ratios predicted by the tripolar mitosis-incomplete cytokinesis model (Fig. 2A).

To compare the two models further, we performed single nucleotide polymorphism (SNP)-based array comparative genomic hybridization analysis of 15 primary WTs, all of which had multiple trisomies and/or multiple segmental imbalances. By calculations based on allele frequencies obtained by the BAF segmentation algorithm (16) we assessed the proportion of cells containing each specific genomic alteration found in every tumor biopsy (Fig. 2D-F; Fig. S5). Sequential acquisition of chromosome alterations would most likely produce genetically distinct populations during tumor development, with the largest clone containing the abnormality acquired first, the second largest the abnormality acquired next *etc*. Such a clonal hierarchy was indeed observed for segmental/structural aberrations in the majority (11/13) of cases with multiple structural imbalances, well in accordance with a previous study showing a sequential acquisition of structural changes in WTs through chromosomal breakage-fusion-bridge cycles (17). In contrast, of the 24 trisomies detected, all but one (+13 in WT-B) were present at frequencies that were identical to the other trisomies present in the same case (P<0.001; trisomies compared to structural changes; Fisher's exact test), indicating that the trisomies in each case

8

were acquired at the same time point in tumor development. To corroborate this pattern with an independent method, we then analyzed chromosome copy numbers by interphase FISH in foci of 30-100 cells in sections from two primary WTs, one of which exhibited trisomy 7 and 12, and the other trisomy 8 and 12. By comparing the number of centromeric FISH signals for these chromosomes to a known disomic reference chromosome, the spatial distribution of trisomic clones could be traced in each tumor (Fig. 3; Fig. S6). In neither case could any focus exhibiting only one of the trisomies be found, as would be expected from the sequential model. Instead, well delimited tumor regions that were trisomic for both of the assayed chromosomes were observed to border directly on areas of disomic tumor cells, again consistent with a concurrent generation of trisomies through as single abnormal mitotic event, as predicted by the tripolar mitosis-incomplete cytokinesis model.

Discussion

Taken together, our data show that an elevated frequency of non-disjunction at bipolar mitosis mediated by a defective SAC is unlikely to explain the occurrence of multiple whole chromosome gains in WT. Instead, a combination of spindle multipolarity and failed cytokinesis appeared to be a strong candidate mechanism. Daughter cells from such asymmetrical cell divisions were capable of again entering mitosis and form novel clones. Our data did not provide information regarding the long-term clonogenic *in vitro* survival of cells having acquired trisomies through this mechanism, but the finding that clones harboring double trisomies could be mapped to confined topographical regions in tumor tissue indicated that at least some daughter cells having acquired concurrent trisomies in WT can expand clonally and contribute to tumor development. Considering the relatively high frequency of baseline chromosome missegregation found in bipolar mitoses (1:50 cell divisions), our model does not exclude that additional whole

9

chromosome gains and losses occur during the expansion of clones with multiple trisomies, leading to an even more complex panorama of chromosome aberrations. Neither does it contradict previous studies showing that polysomic chromosomes are prone to undergo structural rearrangements (18). However, our finding that the multipolar anaphase cells giving rise to trisomies occurred at a very low frequency in each of the studied tumors and that their daughters did not always survive to proliferate further, indicate that the acquisition of trisomies through such mitoses is probably a rare, possibly once-only, phenomenon during the development of a tumor. This could explain why tumor cells only exhibiting trisomies are typically quite stable cytogenetically, showing sub-clones in only a minority of cases. Furthermore, our data indicate that clonal evolution of polysomies occurs through discrete steps in which multiple trisomies may arise, rather than as a continuous process. This is in stark contrast to previously suggested models based on defective control of sister-chromatid separation (1-5), in which gains and losses of chromosomes are more likely to be acquired continuously during tumor cell proliferation. Our suggested model may be of importance for the generation of trisomies also in other tumors frequently showing multiple trisomies and is consistent with studies of allele dosages in pediatric high hyperdiploid acute lymphoblastic leukemias, showing that hyperdiploidy most probably originates in a single aberrant mitosis (19). The present study adds to several other arguing for the importance of centrosome dysregulation for the generation of aneuploidy (10, 20-22), but it is the first to suggest an empirically based mechanism directly linking supernumerary centrosomes and spindle multipolarity to trisomy formation. Furthermore, it is the first to show that multiple chromosome copy number alterations can occur through mitoses that physiologically satisfy the SAC.

Materials and Methods

Short-term cultures established from fibroblasts and primary tumors were sub-cultured no more than five times before analysis. MVA12 exhibited the bi-allelic *BUB1B* mutations 2211-2212insGTTA _S738fsX753 and c.2441G>A_p.R814H (8), whereas MVA41C contained mutation c.2144-2A>G and c.464A>G_ p.Y155C. Cell culture, fixation, FISH, and immunofluorescence were performed as described previously (14). Chromosome segregation was scored by tri-colour FISH in ana-telophase cells using centromeric and single-copy probes (Abbott Molecular, Abbott Park, IL). For holographic time lapse microscopy, the HoloMonitor M2 (Phase Holographic Imaging AB, Lund, Sweden) was used to digitally capture holograms every 2-5 minutes, as described by Mölder *et al.* (23). For time lapse phase-contrast/fluorescence microscopy the NIS Elements Br software (Nikon Instruments Inc., Amsterdam, the Netherlands) was used to acquire images at 5-minute intervals. Detection of genomic imbalances by SNP-array was performed by HumanCNV370-Duo/Quad Genotyping BeadChips (Illumina Inc., San Diego, CA) according to the manufacturer's specifications. A detailed description of the experimental methods can be found on-line (Supporting Text S1).

References

1.   Lengauer C, Kinzler, KW, & Vogelstein, B (1997) Genetic instability in colorectal cancers. *Nature* 386:623-627.

2.   Lengauer C, Kinzler, KW, & Vogelstein, B (1998) Genetic instabilities in human cancers. *Nature* 396:643-649.

3.   Rajagopalan H, et al. (2004) Inactivation of hCDC4 can cause chromosomal instability. *Nature* 428:77-81.

4.   Cahill DP, et al. (1998) Mutations of mitotic checkpoint genes in human cancers. *Nature* 392:300-303.

5.   Barber TD, et al. (2008) Chromatid cohesion defects may underlie chromosome instability in human colorectal cancers. *Proc Natl Acad Sci U S A* 105:3443-3448.

6.   Hernando E, et al. (2001) Molecular analyses of the mitotic checkpoint components hsMAD2, hBUB1 and hBUB3 in human cancer. *Int J Cancer* 95:223-227.

7.   Ru HY, Chen, RL, Lu, WC, & Chen, JH (2002) hBUB1 defects in leukemia and lymphoma cells. *Oncogene* 21:4673-4679.

8.   Hanks S, et al. (2004) Constitutional aneuploidy and cancer predisposition caused by biallelic mutations in BUB1B. *Nat Genet* 36:1159-1161.

9.   Ghadimi BM, et al. (2000) Centrosome amplification and instability occurs exclusively in aneuploid, but not in diploid colorectal cancer cell lines, and correlates with numerical chromosomal aberrations. *Genes Chromosomes Cancer* 27:183-190.

10.   Ganem NJ, Godinho, SA, & Pellman, D (2009) A mechanism linking extra centrosomes to chromosomal instability. *Nature* 460:278-282.

11.	Stewénius Y, et al. (2005) Structural and numerical chromosome changes in colon cancer develop through telomere-mediated anaphase bridges, not through mitotic multipolarity. *Proc Natl Acad Sci U S A* 102:5541-5546.

12.	Rivera MN & Haber, DA (2005) Wilms' tumour: connecting tumorigenesis and organ development in the kidney. *Nat Rev Cancer* 5:699-712.

13.	Graham FL, Smiley, J, Russell, WC, & Nairn, R (1977) Characteristics of a human cell line transformed by DNA from human adenovirus type 5. *J Gen Virol* 36:59-74.

14.	Gisselsson D, et al. (2008) When the genome plays dice: circumvention of the spindle assembly checkpoint and near-random chromosome segregation in multipolar cancer cell mitoses. *PLoS ONE* 3:e1871.

15.	Bylund L, Kytola, S, Lui, WO, Larsson, C, & Weber, G (2004) Analysis of the cytogenetic stability of the human embryonal kidney cell line 293 by cytogenetic and STR profiling approaches. *Cytogenet Genome Res* 106:28-32.

16.	Staaf J, et al. (2008) Segmentation-based detection of allelic imbalance and loss-of-heterozygosity in cancer cells using whole genome SNP arrays. *Genome Biol* 9:R136.

17.	Stewénius Y, et al. (2007) Defective chromosome segregation and telomere dysfunction in aggressive Wilms' tumors. *Clin Cancer Res* 13:6593-6602.

18.	Kost-Alimova M, Fedorova, L, Yang, Y, Klein, G, & Imreh, S (2004) Microcell-mediated chromosome transfer provides evidence that polysomy promotes structural instability in tumor cell chromosomes through asynchronous replication and breakage within late-replicating regions. *Genes Chromosomes Cancer* 40:316-324.

19.	Paulsson K, et al. (2003) Formation of trisomies and their parental origin in hyperdiploid childhood acute lymphoblastic leukemia. *Blood* 102:3010-3015.

20.   Ghadimi BM, et al. (2000) Centrosome amplification and instability occurs exclusively in aneuploid, but not in diploid colorectal cancer cell lines, and correlates with numerical chromosomal aberrations. *Genes Chromosomes Cancer* 27:183-190.

21.   Saunders WS, et al. (2000) Chromosomal instability and cytoskeletal defects in oral cancer cells. *Proc Natl Acad Sci USA* 97:303-308.

22.   Silkworth WT, Nardi, IK, Scholl, LM, & Cimini, D (2009) Multipolar spindle pole coalescence is a major source of kinetochore mis-attachment and chromosome mis-segregation in cancer cells. *PLoS One* 4:e6564.

23.   Mölder A, et al. (2008) Non-invasive, label-free cell counting and quantitative analysis of adherent cells using digital holography. *J Microsc* 232:240-247.
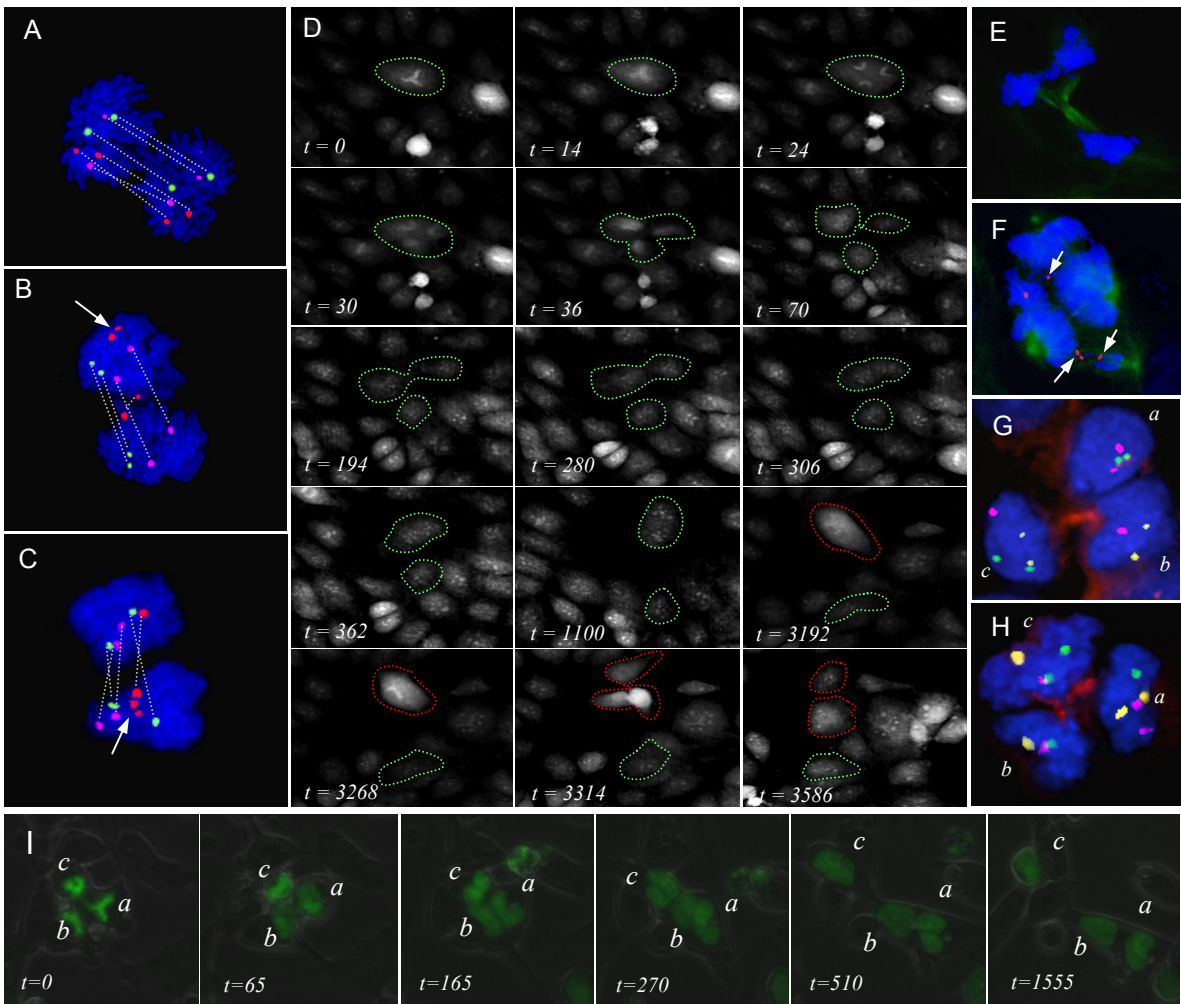
Figure Legends

Figure 1. Chromosome missegregation in bipolar and multipolar mitoses. *(A)* FISH with centromeric probes for chromosomes 7 (red), 12 (green) and 18 (violet) shows amphitelic chromosome segregations at anaphase in an F-N fibroblast. Homologous chromosomes equidistant from the cellular equator have been classified in probable sister chromosome pairs (broken white lines). *(B, C)* Probes for chromosomes 13 (green), 18 (violet) and 21 (red) shows 3-1 missegregation at telophase of chromosome 21 (arrows) in an F-N fibroblast (B) and an MVA28 fibroblast (C). *(D)* Time-lapse series (*t* is time in minutes*)* showing a tripolar metaphase (green broken lines; *t* = 0) followed by tripolar ana-telophase (*t* = 14-36 min). Cytokinesis is initiated along two cleavage furrows in this cell division (*t* = 70 min), but one of the cleavage furrows regresses and only two daughter cells are formed (*t* = 306 min), of which the larger is binucleate as evidenced by two clusters of nucleoli. The larger cell (*t* = 3192 min) enters mitoses (red broken lines), forming a single mitotic plate and divides into two daughters (*t* = 3586 min). Daughter cells from both cell divisions remained without evidence of cell death or degeneration throughout the observation time (139 h total time lapse; Video S1). *(E, F)* Immunofluorescence staining for beta tubulin (green) and MAD2L1 (red) in WiT49 cells shows retention of MAD2L1 foci in a complex tetrapolar anaphase cell with lagging chromosomes (*F*, arrows), while no MAD2L1 foci are present in a tripolar anaphase cell (*E*); note the absence of a beta tubulin positive midbody between the two upper poles in *E. (G)* Immunofluorescence staining for beta tubulin (red) combined with FISH for the centromeres of chromosomes 4 (green), 7 (violet), and 9 (yellow) in a post-mitotic HEK293D cell shows 3-1 segregation of chromosome 7, resulting in trisomy 7 in the binucleated daughter cell (nuclei *a* and *b*) and monosomy in the mononucleated daughter cell (*c*). (*H*) Beta tubulin staining combined with FISH for the centromeres of
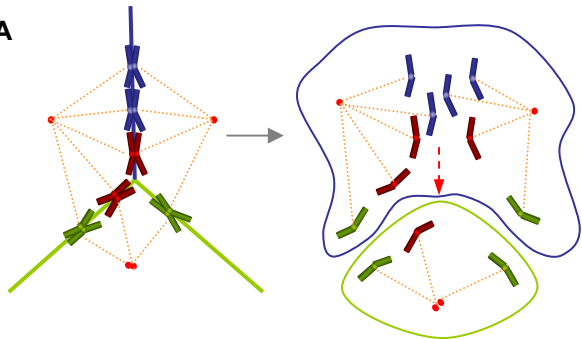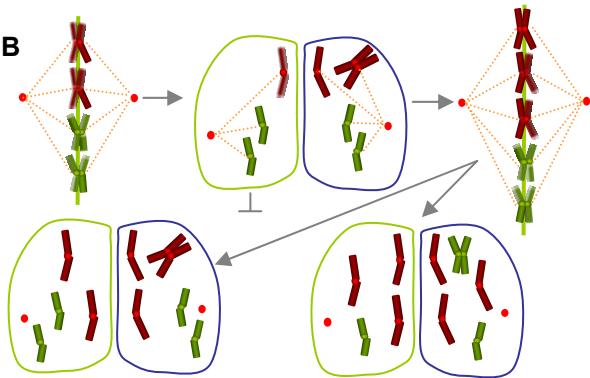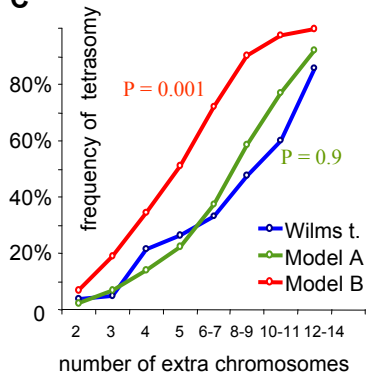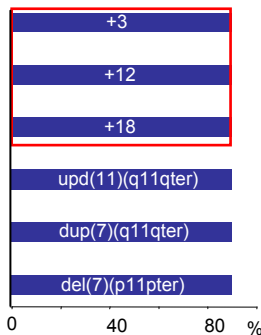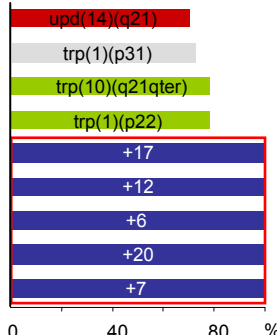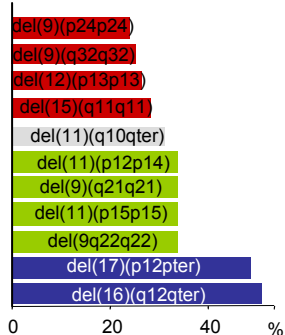
15

chromosomes 3 (yellow), 11 (violet), and 15 (green) in a telophase HEK293D cell shows

concurrent formation of trisomies for chromosomes 3 and 11 in the binucleated daughter cell

(nuclei *a* and *b*) and monosomies for these chromosomes in the mononucleated daughter cell (*c*);

note the absence of midbody between *a* and *b*. (*I*) Time-lapse fluorescence/phase contrast

microscopy in HEK293D *H2B-GFP* cells shows a tripolar anaphase (*t*=0) resulting in one

binucleated (*a, b*) and one mononucleated (*c*) daughter cell (*t*=1555 min; Video S3).

Figure 2. Models for the generation of trisomies and tetrasomies. *(A)* A tripolar nuclear

division with amphitelic sister chromatid separation and segregation, followed by incomplete

cytokinesis will generate tetrasomies in one daughter cell (blue membrane, right) for

chromosomes (blue) of which both homologues are located on the metaphase axis (blue line, left)

along which the cleavage furrow fails to ingress completely (red arrow, right), while trisomies

will be generated in the same daughter cell for homologues (red) located on this axis and on

either of the other axes (green lines, left); disomies will be retained when both homologues

(green) are present on the axes (green) along which cytokinesis is complete. *(B)* A bipolar mitosis

with missegregation of one chromosome (red) will generate one trisomic and one monosomic

daughter cell. Another missegregation event in the trisomic cell population involving the same

(red) chromosome will result in tetrasomic and disomic daughter cells (lower left), while

missegregation involving another chromosome will result in two trisomies (lower right). *(C)* The

frequency of tetrasomic tumors (blue plot) in 152 WTs with at least two whole chromosome gains

is well in accordance with the model in Fig. *2A* (green plot) but differs significantly (Chi Square

test) from the distribution predicted from the model in Fig. *2B* (red plot). *(D-F)* The proportion of

cells carrying specific chromosomal imbalances in primary WT biopsies WT-F (D), WT-G (E),

and WT-H (F), estimated from B-allele frequencies at SNP-array analysis. Trisomies (+) are
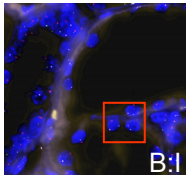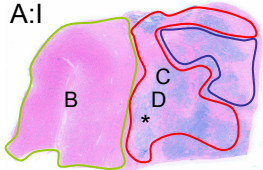
16

present in an equal proportion of cells (*D* and *E*; red demarcations), while segmental imbalances are typically present in clones of different sizes (*E* and *F*). Abnormalities present at similar proportions are signified by identical colors (red, green or blue bars), while abnormalities present in significantly different proportions of cells are signified by different colors. Grey bars indicate populations for which the proportion confidence intervals overlapped with that of at least one other population. Abbreviations: del, hemizygous deletion; dup, duplication; trp, triplication; upd, uniparental disomy.

Figure 3. Spatial distribution of trisomic cells in tumor tissue. *(A)* Tissue section from WT-G with trisomies 7 and 12 in a sub-population of tumor cells, previously detected by SNP-based array comparative genomic hybridization. Most nuclei (stained by diaminophenylindol, blue) are sectioned, leading to a reduced number of probe signals. Therefore, the distribution of trisomic cells was mapped by calculating copy number ratios in foci of 30-100 cells by FISH with centromeric probes for chromosomes 7 (*A:II*) and 12 (*A:III*), using centromere 16 as a reference for disomy (see Fig. S6E for signal number ratios). This allowed demarcation of areas containing cells with trisomies (red borders in *A:I*) and disomies (blue borders) in the corresponding haematoxylin-eosin section. Blue and red filled circles in *A:II* and *A:III* indicate cell populations classified as disomic and trisomic, respectively. The adjacent normal kidney (green borders) contains only disomic areas. The asterisk represents disomic stromal tissue surrounding a blood vessel. *(B)* Representative FISH image of normal kidney tubules (area *B* in *A:I*; rectangular area in *B:I* is shown at higher magnification in *B:II*) with disomy for chromosomes 7 (red), 12 (green) and 16 (violet; arrow in *B:II*). *(C, D)* Trisomic cells were detected in epithelial (*C* in *A:I*) and stromal (*D* in *A:I*) tumor elements, as exemplified by cells showing three signals for each of chromosomes 7 and 12 (arrows in high-power images *C:II* and *D:II*).

A

B

C

frequency of tetrasomy

P = 0.001

P = 0.9

- Wilms t.
- Model A
- Model B

number of extra chromosomes

D

- +3
- +12
- +18
- upd(11)(q11qter)
- dup(7)(q11qter)
- del(7)(p11pter)

E

- upd(14)(q21)
- trp(1)(p31)
- trp(10)(q21qter)
- trp(1)(p22)
- +17
- +12
- +6
- +20
- +7

F

- del(9)(p24p24)
- del(9)(q32q32)
- del(12)(p13p13)
- del(15)(q11q11)
- del(11)(q10qter)
- del(11)(p12p14)
- del(9)(q21q21)
- del(11)(p15p15)
- del(9q22q22)
- del(17)(p12pter)
- del(16)(q12qter)
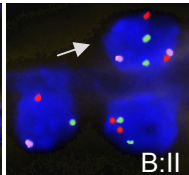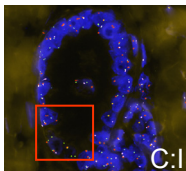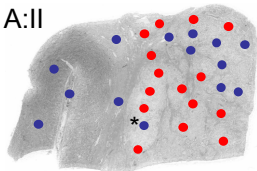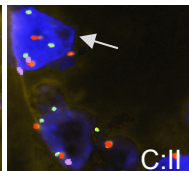
Legends to Supporting Information

Table S1. Frequency of chromosome segregation errors in anaphase cells.

Figure S1. **FISH and immunofluorescence.** *(A)* FISH with probes for the centromeres of chromosomes 7 (red), 12 (green) and 18 (violet) shows amphitelic chromosome segregations at anaphase in an F-N fibroblast. Homologous chromosomes equidistant from the cellular equator have been classified in probable sister chromosome pairs (broken white lines). *(B)* Immunofluorescence for Aurora kinase A for the detection of active centrosomes (red-orange) combined with FISH for the centromere of chromosome 18 (violet) shows lagging of a chromosome 18 homologue in a bipolar mitosis in MVA28. *(C)* Immunofluorescence for beta tubulin (red) combined with FIS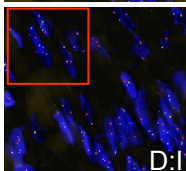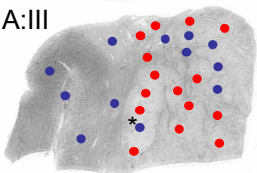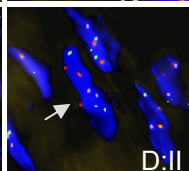H for the centromere of chromosome 12 (green) shows a tripolar ana-telophase cell having undergone 4-3-1- segregation in WiT49; no midbody has yet formed. *(D, E)* Labeling as in *C* shows 3-1 segregations in a telo-interphase cells after tripolar nuclear division followed by incomplete cytokinesis, as evidenced by a the presence of three nuclei and a single midbody (arrows). *(E)* Immunofluorescence staining for beta tubulin (green) and MAD2L1 (red) shows multiple centromeric MAD2L1 foci at metaphase in a tetrapolar mitosis in WiT49 as an indication of maintained spindle assembly checkpoint activity.

Figure S2. **Data from holographic imaging.** *(A)* Summary of time-lapse digital holographic imaging of 50 bipolar anaphase WiT49 cells and their daughter cells. Of these, 47 underwent complete cytokinesis (blue lines) while the remaining exhibited regression of the cleavage furrow resulting in binucleate daughter cells (green lines). Only one daughter cell underwent cell death during the observation period (orange line). Arrows indicate that the monitored cells were viable

at the end of the time-lapse series, whereas perpendicular lines denote cell death as evidenced by pyknosis, karyorrhexis, and detachment. *(B)* Summary of time-lapse imaging of tripolar anaphase WiT49 cells and their daughter cells. Incomplete cytokinesis with ingression of the cleavage furrow along a single plane is marked by red lines; other annotations are as in *A*. The total rate of cytokinetic failure, including both complete failure and single-furrow cytokinesis, was 15-fold higher in multipolar than in bipolar anaphase cells (P<0.0001; Fisher's exact test). Of the totally 35 daughter cells of tripolar anaphase cells that could be followed for 24 hours or more, 9% subsequently underwent death or degeneration, compared to 1% (1/99) daughter cells from bipolar anaphase cells. *(C)* Time-lapse digital holographic imaging (*t* is time in minutes) of the cytoplasmic border in a tripolar cell division, showing initial formation of two cleavage furrows of which one undergoes complete ingression whereas the other regresses (arrow); note that the focal plane has been adjusted to visualize cytoplasmic borders, resulting in less clear visualization of the metaphase plate (*t*=0).

Figure S3. Time-lapse fluorescence/phase contrast microscopy. Mitotic divisions in HEK293D *H2B-GFP* cells. Chromatin is visible in green fluorescence and cytoplasmic borders are discerned in phase contrast; *t*=time in minutes. *(A)* Bipolar mitosis followed by complete cytokinesis resulting in two cells, each with one daughter nucleus (*a* and *b*; Video S2). *(B)* Tripolar mitosis followed by incomplete cytokinesis resulting in one binucleated (*a*, *b*) and one mononucleated (*c*) daughter cell (Video S4). *(C)* Tripolar anaphase followed by complete cytokinesis resulting in three mononucleated daughter cells (*a*, *b*, and *c*; Video S5).

Figure S4. Data from fluorescence/phase contrast microscopy and FISH-based segregation analysis. Summary of real-time monitoring of daughter cells resulting from *(A)* 20 bipolar and

(B) 10 tripolar mitoses in the HEK293D *H2B-GFP* cells. Each cell division was monitored from metaphase or anaphase at 5-minute intervals until the number of separate daughter cells could be clearly discerned, typically for 12-24 h. Ideograms of daughter cell configurations are shown along the Y axes, with nuclei in green and cytoplasm in grey. *(C)* Summary of segregation patterns of originally disomic chromosomes, scored in telophase nuclei in daughter cells resulting from bipolar mitosis and complete cytokinesis according to parallel beta tubulin staining for midbody configurations. *(D)* Corresponding segregation patterns in daughter cells resulting from tripolar mitosis and incomplete cytokinesis. Ideograms of daughter cell configurations are shown along the Y axes, with nuclei in green, cytoplasm in grey, and centromeric probe copy numbers in yellow. Data were produced by pooling results from centromeric probes for chromosomes 3, 4, 7, 9, 11, and 15. There was no difference in the segregation patterns observed among these chromosomes (P>0.05; Fisher's exakt test).

Figure S5. **Proportion of tumour cells with numerical and segmental genomic imbalances.** Proportion of cells carrying specific chromosome abnormalities were estimated from B-allele frequencies. Differently coloured bars indicate significant differences in the proportion of cells as described in the legend to Fig. 2; grey bars indicate genomic imbalances at proportions that could not be distinguished statistically from imbalances with similar frequency estimates. Trisomies are signified by +, and monosomies by – signs; dup, duplication; del, hemizygous deletion; upd, uniparental disomy.

Figure S6. Localization of aneuploid cells in tumour tissue. (*A*, *B*) Two sections from the Wilms tumour WT-T, analysed and annotated as in Fig. 3, with trisomies of chromosomes 8 (*A:II* and *B:II*) and 12 (*A:III* and *B:III*) in tumour foci (red circles) located centrally in the tumour (red

borders in *A:I* and *B:I)*, sharply demarcated from disomic cell populations (blue circles, blue borders) in the periphery of the tumour adjacent to non-neoplastic kidney (green borders in *A:I*). *(C)* The signal number ratios (SNRs) from centromeric probes for chromosomes (chr) 8 and 12 compared to chromosome 10 (disomic control) in WT-T section *A* are close to 1 in normal kidney (green column) and in the tumour region demarcated by blue borders in *A:I*, (blue column) corresponding to disomy for both chromosomes 8 and 12. In contrast, the SNR for these chromosomes is close to 3:2 (1.5) in the red-bordered region in *A:I* (red column), corresponding to trisomy for both chromosomes. Error bars correspond to standard deviation in pooled data from all analyzed foci within the respective regions. *(D)* SNRs obtained from all analyzed foci in WT-T section *B*, corresponding to disomy for chromosomes 8 and 12 in the blue-bordered region (blue bar) and trisomy for both chromosomes in the red-bordered region (red bar) in *B:I*. *(E)* SNRs from all analyzed foci in WT-G (Fig. 3), showing disomy for chromosomes 7 and 12 in normal kidney (green columns, green borders in Fig. 3 A:I) and in the blue-bordered tumour region (blue columns), while both chromosomes are trisomic in the red-bordered region (red columns).

Video S1. **Tripolar mitosis and incomplete cytokinesis by time lapse phase holographic microscopy.** The video shows tripolar metaphase followed by tripolar ana-telophase in the WiT49 cell line. Two of the three daughter nuclei ultimately segregate to the same daughter cell, which subsequently undergoes mitosis to form two new daughter cells. Daughter cells from both cell divisions remained without evidence of cell death or degeneration throughout the observation time (139 h total time lapse). Video *S1A* corresponds to a greyscale rendering of the entire image field. The movie corresponds to still images in Fig. *1D*. Video *S1B* has been cropped to focus on events in the binucleate daughter cell. Here, colours have been used to illustrate optical density

(low-high = red-blue). Cytoplasmic membranes are typically observed in red-orange, interphase nuclei in yellow-green, and mitotic cells in green-blue. Note that also non-mitotic cells undergoing spheroid transformation attain green-blue colour.

Video S2. Bipolar mitosis by time lapse fluorescence/phase contrast microscopy. The video shows bipolar mitosis followed by complete cytokinesis in the HEK293D *H2B-GFP* line (8 h total time lapse).

Videos S3 and S4. Tripolar mitosis and incomplete cytokinesis by time lapse fluorescence/phase contrast microscopy. The videos show tripolar cell divisions followed by incomplete cytokinesis resulting in one mononucleated and one binucleated daughter cell, respectively for each mitosis, in the HEK293D *H2B-GFP* line (28h and 24 h total time lapse for S3 and S4, respectively).

Video S5. Tripolar mitosis and complete cytokinesis by time lapse fluorescence/phase contrast microscopy. The video shows tripolar anaphase followed by complete cytokinesis resulting in three mononucleated daughter cells in the HEK293D *H2B-GFP cell line* (20 h total time lapse).

Supporting Dataset S1. SNP-array segments. Segmented SNP-array data provided in Microsoft Excel format. Constitutional variants and other patient-specific genotype information have been excluded to prevent the identification of individual patients. Segments were identified by the BAF segmentation algorithm as outlined in Materials and Methods.

Supporting text S1. Materials and methods. Detailed description including references.

Table S1. Frequency of chromosome segregation errors in anaphase cells

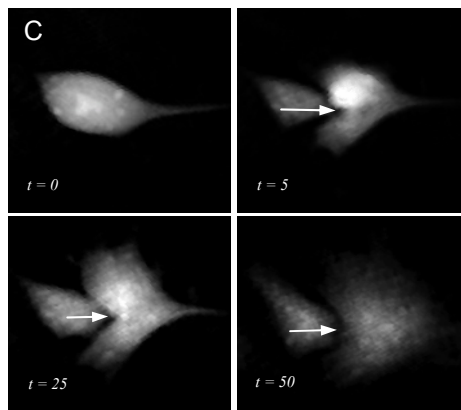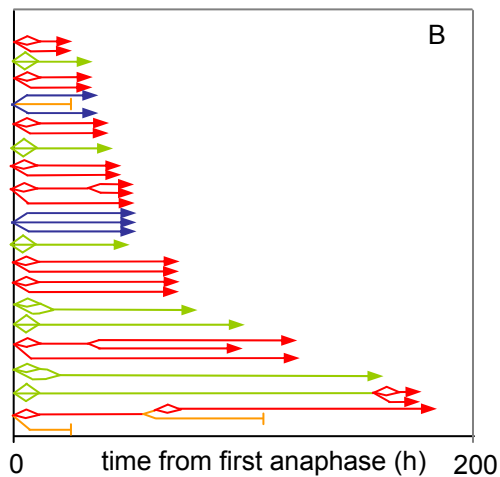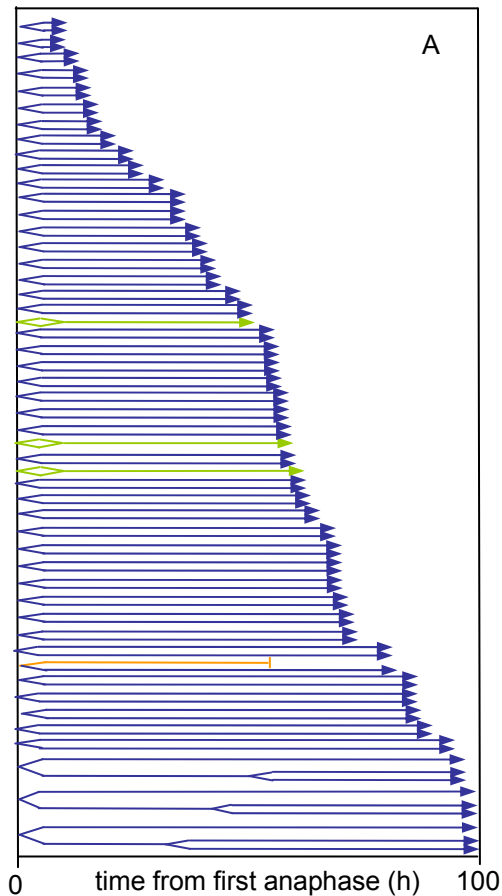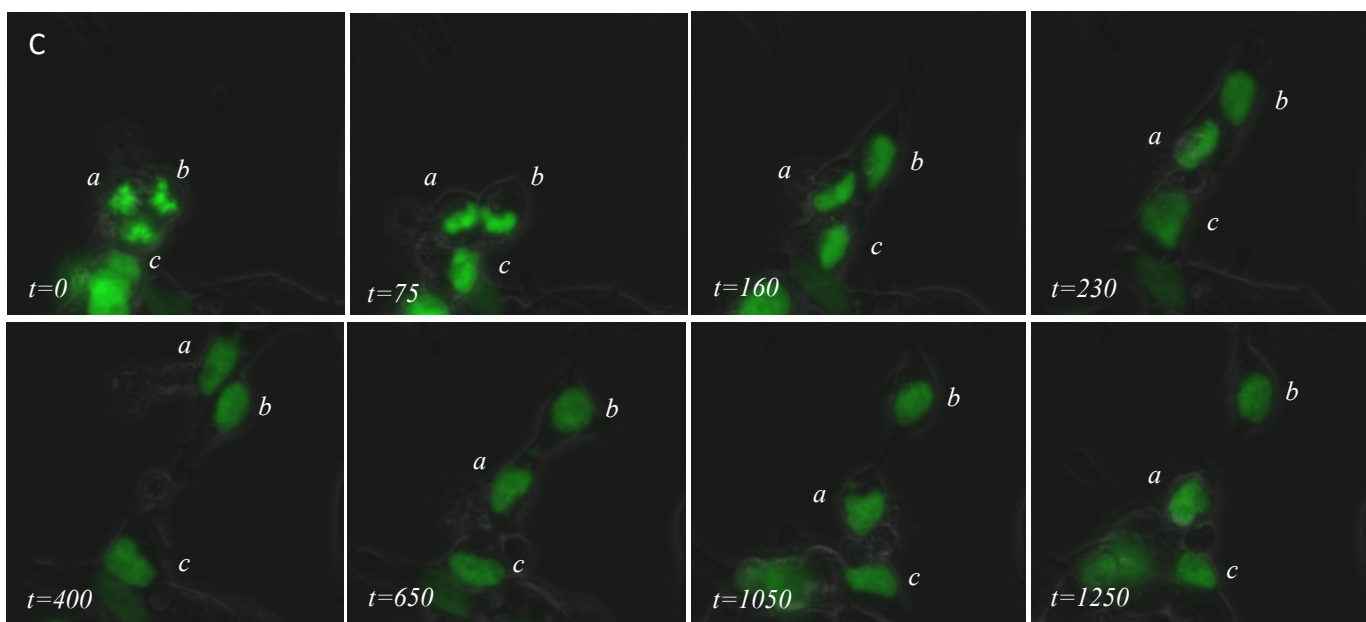| Cell type	Whole chr. gains[1]	Missegregation/chr/mitosis (bipolar anaphase)[4]	Missegregation/chr/mitosis (multipolar anaphase)
Normal fibroblasts			
F-I	none	3.9×10^{-4}	0
F-J	none	3.3×10^{-4}	0
F-K	none	4.1×10^{-4}	0
F-N	none	4.1×10^{-4}	0
SAC deficient fibroblasts			
MVA12	n/a[2]	5.1×10^{-3}	0
MVA28	n/a	5.9×10^{-3}	0
MVA41	n/a	4.8×10^{-3}	0
SAC deficient cancer cell lines			
SW480	2,11,13,21	3.6×10^{-3}	4.0×10^{-2}
LoVo	5,7,12	1.5×10^{-3}	4.0×10^{-2}
SAC proficient cancer cell line			
DLD1	20 (subclonal)	5.0×10^{-4}	6.6×10^{-3}
Wilms tumour cells			
WiT49	6,12,19	6.4×10^{-4}	3.3×10^{-2}
WT-A	1,2,5,6,**7**,8,10,**18**	$0\text{-}6.7 \times 10^{-4}$	4.2×10^{-2}
WT-B	8,13,**18**	5.0×10^{-4}	9.0×10^{-3}
WT-C	**12**,13,20,21	6.0×10^{-4}	1.7×10^{-2}
WT-D	8,16[3]	$0\text{-}1.2 \times 10^{-3}$	1.7×10^{-2}
WT-E	**7**,8,**12**,13	5.0×10^{-4}	7.8×10^{-3}

[1]Chromosomes used to identify neoplastic cells in primary Wilms tumour biopsies are in bold type; only cell divisions trisomic for these chromosomes were included in the analyses. [2] n/a, not analysed. [3]Monosomy 12 was used to identify neoplastic cells in this case. [4]No missegregation events in bipolar cell divisions were found in cases where intervals are given; the higher value is an estimation of the highest frequency possible, calculated as 1/(total number of scored segregations). Frequencies were based on FISH with centromeric probes for chromosomes 7, 12, and 18, in all cases, complemented with single-copy probes for 13q and 21q for fibroblasts.

A

time from first anaphase (h)
0   100

B

time from first anaphase (h)
0   200

C

t = 0

t = 5

t = 25

t = 50
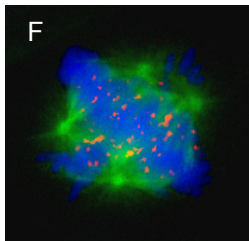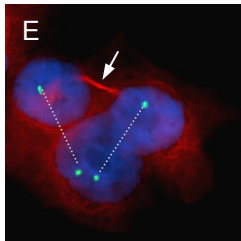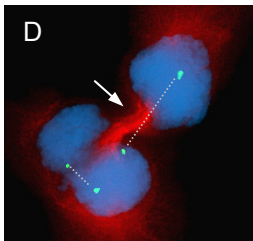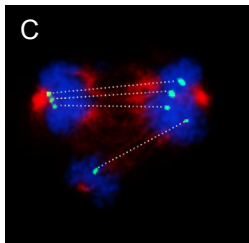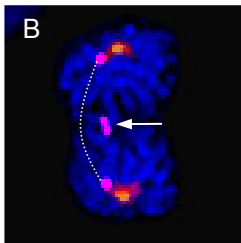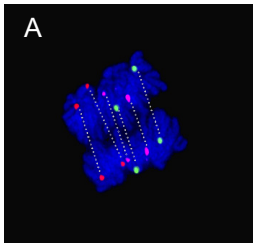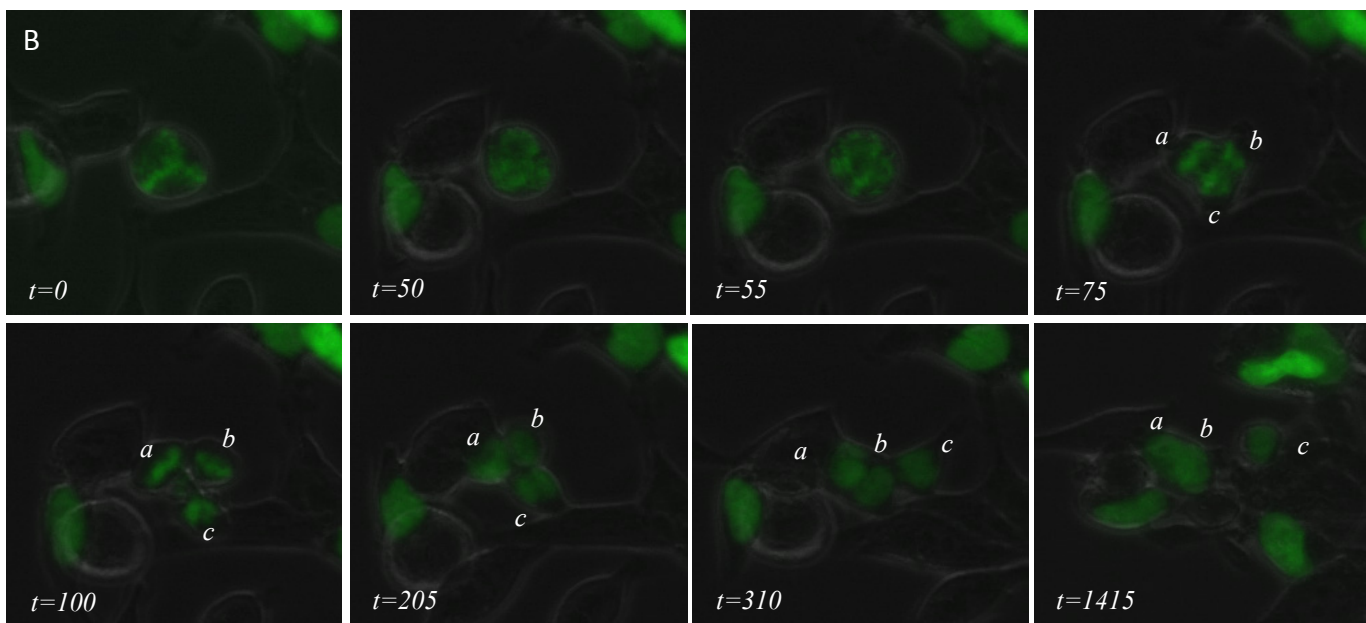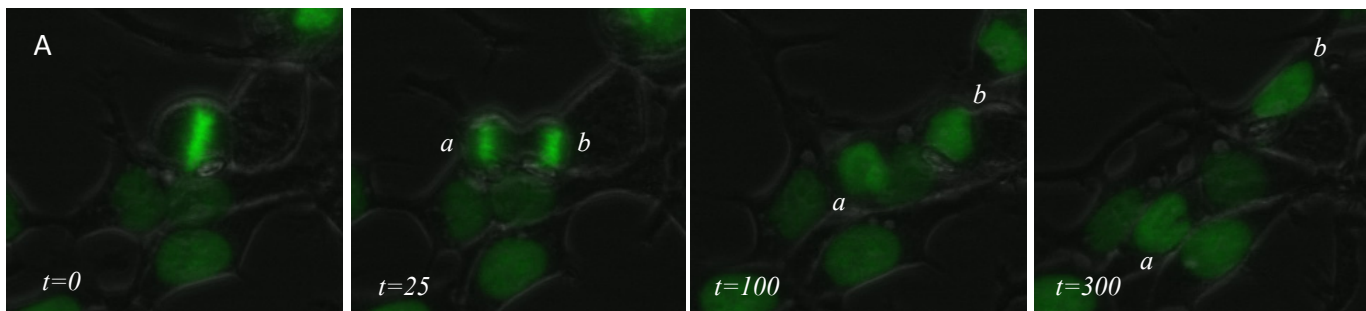
A — Daughter cells - bipolar anaphase
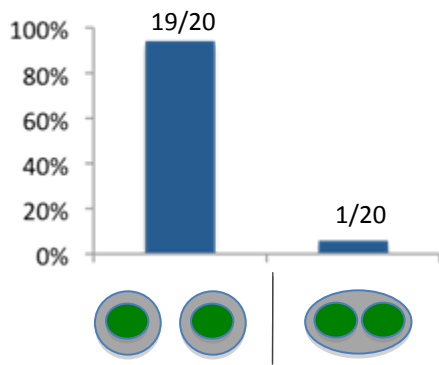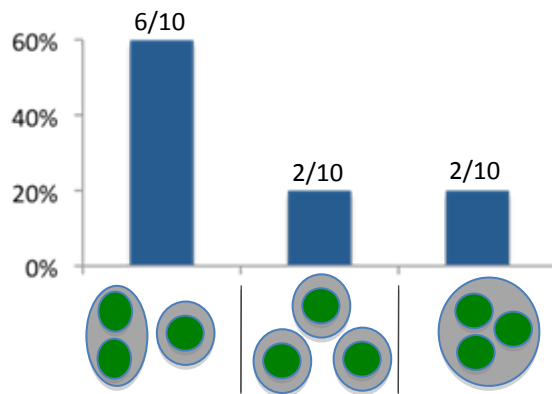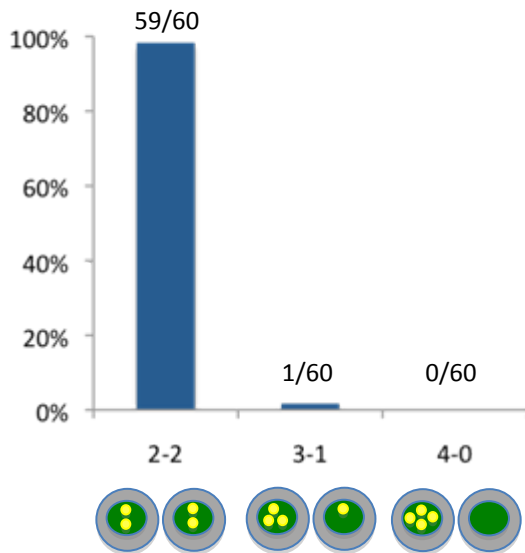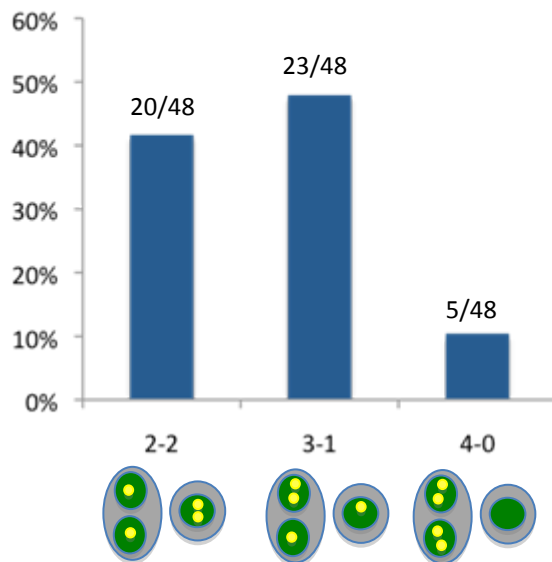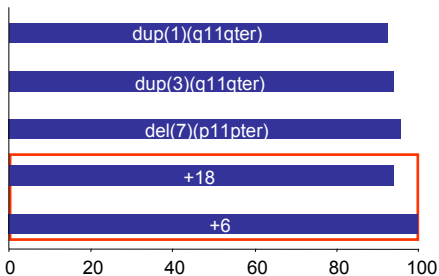B — Daughter cells - tripolar anaphase
C — Chromosome segregation - bipolar telophase/two daughter cells -
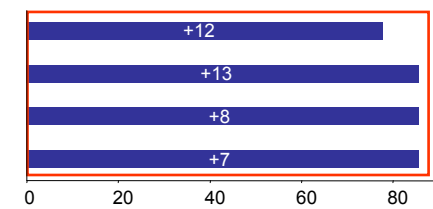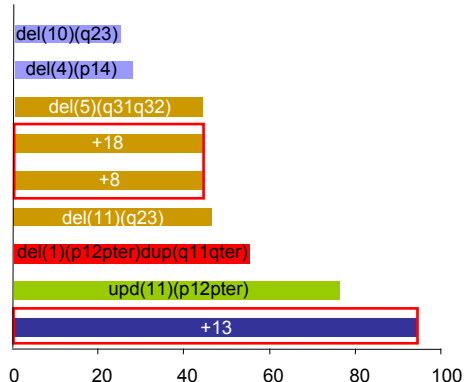D — Chromosome segregation - tripolar telophase/two daughter cells -
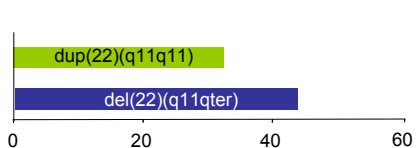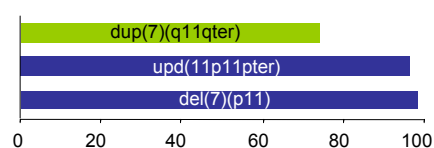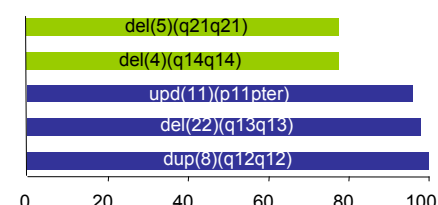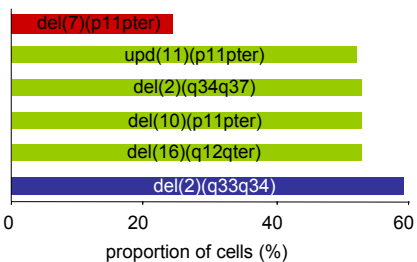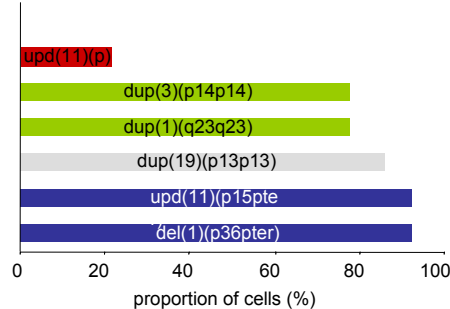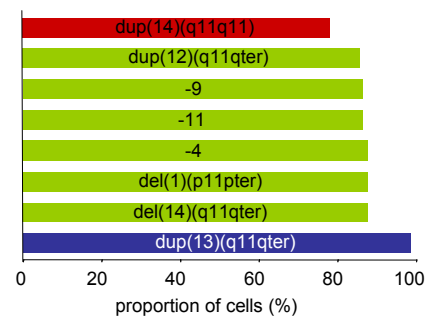
A:I

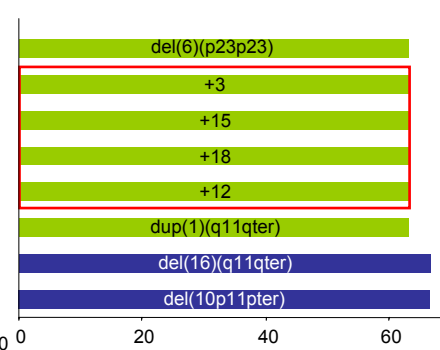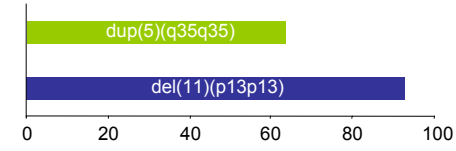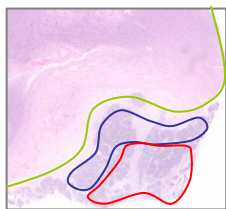**B:I**

A:II

B:II

A:III

B:III

C WT-T (A)

D WT-T (B)

E WT-G
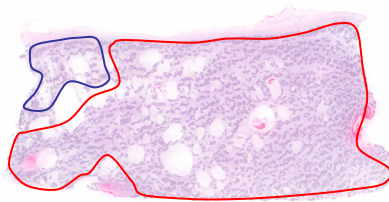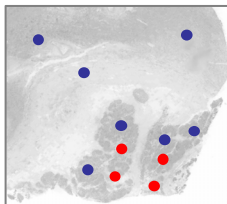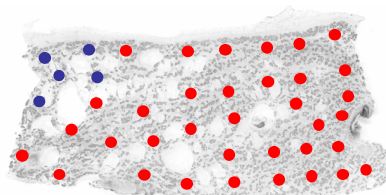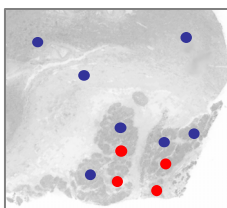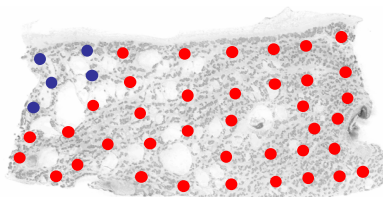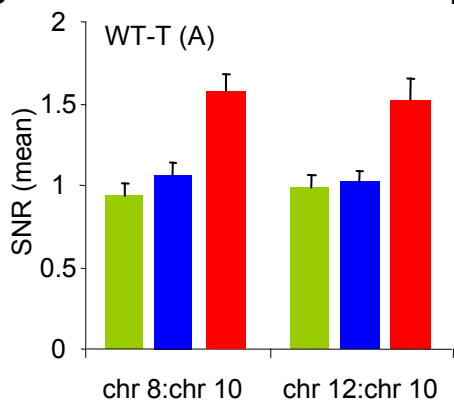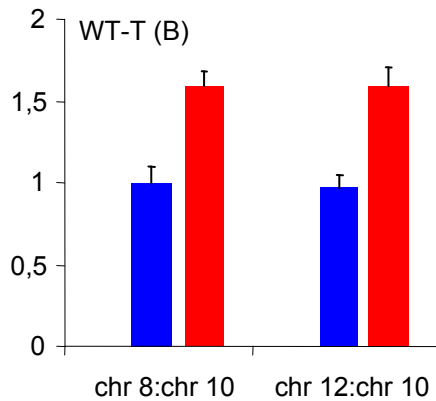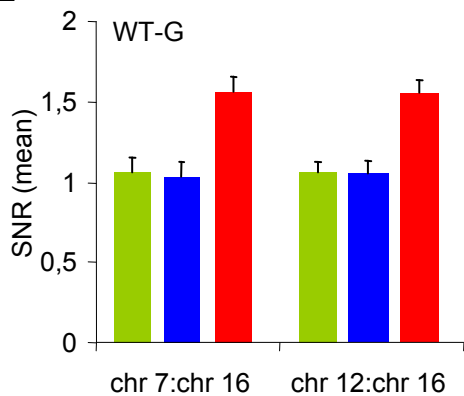
Sample	Chromosome	Genomic Start	Genomic End	Start SNP	End SNP	Size of segment	Median mi	Median Lo	Heterozyg	UCSC seg	Classificati	Fused (3)	Notes
WT_H	9	194201	5516124	rs1096413	rs4237162	5321924	0.56	-0.09	0.3	http://geno	LOSS	No	(1) Proportion of heterozygous SNPs within the defined segment
WT_H	9	80220582	85989847	rs7875946	rs1932654	5769265	0.6	-0.09	0.36	http://geno	LOSS	Yes	(2) Type of allelic imbalance: CNNI; LOSS, loss of genomic material; GAIN, gain of genomic materia
WT_H	9	95717228	95912972	rs1099297	rs1099305	195745	0.6	-0.02	0.5	http://geno	CNNI	No	(3) Indicates whether a segment have been formed by two or more segments.
WT_H	9	1,14E+08	1,15E+08	rs7875641	rs3750534	1224296	0.57	-0.1	0.37	http://geno	LOSS	No	
WT_H	11	194228	8635592	rs1045454	rs2316901	8441365	0.6	-0.09	0.35	http://geno	LOSS	No	
WT_H	11	10360153	19932895	rs2198009	rs2585780	9572743	0.6	-0.08	0.29	http://geno	LOSS	No	
WT_H	11	27749467	40185227	rs1491872	rs1257536	12435761	0.6	-0.12	0.3	http://geno	LOSS	No	
WT_H	11	46923384	1,34E+08	rs2903517	rs528420	87344967	0.59	-0.11	0.32	http://geno	LOSS	Yes	
WT_H	16	45471923	88668856	rs1293061	rs1292593	43196934	0.67	-0.13	0.33	http://geno	LOSS	No	
WT_H	17	53011	15911407	rs1136388	rs3785628	15858397	0.66	-0.1	0.32	http://geno	LOSS	No	
WT_I	1	1,44E+08	1,85E+08	rs1079764	rs1203803	40741317	0.73	0.39	0.32	http://geno	GAIN	No	
WT_I	1	1,85E+08	1,96E+08	rs1048939	rs3790380	10648359	0.75	0.49	0.32	http://geno	GAIN	No	
WT_I	1	1,96E+08	2,47E+08	rs1080160	rs9727917	51560439	0.74	0.41	0.31	http://geno	GAIN	No	
WT_I	3	90525615	1,99E+08	rs2316653	rs7431003	1,09E+08	0.66	0.27	0.34	http://geno	GAIN	Yes	
WT_I	6	165549	1,71E+08	rs6932895	rs6928843	1,71E+08	0.67	0.27	0.32	http://geno	GAIN	Yes	
WT_I	7	193878	56572775	rs1027420	rs1906626	56378898	0.96	-0.45	0.2	http://geno	LOSS	No	
WT_I	18	103671	75758307	rs8091568	rs1108157	75654636	0.66	0.29	0.32	http://geno	GAIN	Yes	
WT_K	7	162448	1,59E+08	rs3924854	rs428183	1,58E+08	0.65	0.22	0.33	http://geno	GAIN	Yes	
WT_K	8	166818	1,46E+08	rs2003497	rs6599560	1,46E+08	0.65	0.23	0.33	http://geno	GAIN	Yes	
WT_K	12	116089	1,32E+08	rs2368834	rs7975069	1,32E+08	0.64	0.22	0.33	http://geno	GAIN	Yes	
WT_K	13	18108426	1,14E+08	rs4293225	rs7324447	95799671	0.65	0.22	0.34	http://geno	GAIN	Yes	
WT_R	1	908247	6717817	rs1330311	rs447558	5809571	0.93	-0.3	0.34	http://geno	LOSS	No	
WT_R	1	1,54E+08	1,55E+08	rs1052067	rs4399146	507438	0.64	0.22	0.45	http://geno	GAIN	No	
WT_R	3	64683154	65128188	rs4132228	rs931234	445035	0.64	0.29	0.3	http://geno	GAIN	No	
WT_R	11	193788	1960117	rs2280543	rs217704	1766330	0.96	0.09	0.21	http://geno	CNNI	No	
WT_R	11	2152557	46232648	rs1074315	rs4426109	44080092	0.6	0.01	0.34	http://geno	CNNI	No	
WT_R	19	18619255	19083070	rs889362	rs1041797	463816	0.65	0.34	0.5	http://geno	GAIN	No	
WT-B	1	751010	1,2E+08	rs3115850	rs6428843	1,19E+08	0.81	-0.08	0.33	http://geno	LOSS	Yes	
WT-B	4	37212514	38617025	rs2380737	rs6531684	1404512	0.62	-0.14	0.38	http://geno	LOSS	No	
WT-B	5	1,36E+08	1,46E+08	rs2188469	rs322468	9892173	0.81	-0.29	0.31	http://geno	LOSS	No	
WT-B	6	0	1,71E+08	rs9321768	rs2518201	1,71E+08	0.58	0.25	0.25	http://geno	GAIN	No	
WT-B	8	211671	1,46E+08	rs1720652	rs2979109	1,46E+08	0.65	0.2	0.36	http://geno	GAIN	Yes	
WT-B	10	96599054	96759759	rs1322181	rs1934975	160706	0.58	-0.1	0.41	http://geno	LOSS	No	
WT-B	11	316564	48289936	rs1124606	rs1483121	47973373	0.94	0.01	0.3	http://geno	CNNI	No	
WT-B	11	1,18E+08	1,19E+08	rs498872	rs4301800	542154	0.78	-0.28	0.45	http://geno	LOSS	No	
WT-B	13	18108426	1,14E+08	rs4293225	rs7999630	95974158	0.7	0.35	0.34	http://geno	GAIN	Yes	
WT-B	18	2842	76069787	rs1085328	rs7243052	76066946	0.63	0.2	0.34	http://geno	GAIN	No	
WT-B	22	15474749	49518559	rs2096537	rs756638	34043810	0.57	0.17	0.33	http://geno	GAIN	Yes	
WT-F	3	41894	1,99E+08	rs9681213	rs1015490	1,99E+08	0.65	0.24	0.34	http://geno	GAIN	No	
WT-F	7	149081	61631605	rs7806592	rs6651049	61482525	0.9	-0.36	0.35	http://geno	LOSS	No	
WT-F	7	61673005	1,59E+08	rs2123572	rs6979985	96967051	0.65	0.23	0.33	http://geno	GAIN	No	
WT-F	11	189256	46254207	rs3741411	rs1043765	46064952	0.94	0.03	0.34	http://geno	CNNI	No	
WT-F	12	64079	1,32E+08	rs4980929	rs7975069	1,32E+08	0.65	0.21	0.33	http://geno	GAIN	Yes	
WT-F	18	277705	76116152	rs8088001	rs1296063	75838448	0.67	0.19	0.34	http://geno	GAIN	No	
WT-G	1	68358601	69180398	rs1367452	rs1274006	821798	0.71	0.38	0.27	http://geno	GAIN	No	
WT-G	1	90896251	91695842	rs1080182	rs1205880	799592	0.72	0.37	0.46	http://geno	GAIN	No	
WT-G	1	1,08E+08	1,15E+08	rs1235415	rs1989138	6895772	0.72	0.35	0.59	http://geno	GAIN	Yes	
WT-G	1	1,16E+08	2,47E+08	rs552279	rs9727917	1,31E+08	0.72	0.37	0.33	http://geno	GAIN	Yes	
WT-G	6	112510	1,7E+08	rs1220945	rs1219223	1,7E+08	0.67	0.26	0.33	http://geno	GAIN	Yes	
WT-G	7	149081	1,59E+08	rs7806592	rs4909047	1,59E+08	0.67	0.27	0.34	http://geno	GAIN	No	
WT-G	8	180568	51492279	rs1048836	rs1481471	51311711	0.67	0.28	0.29	http://geno	GAIN	Yes	
WT-G	8	55029044	55918810	rs6981243	rs1873963	889767	0.65	0.27	0.34	http://geno	GAIN	No	
WT-G	8	55923678	60909551	rs1095843	rs6471835	4985874	0.56	0.51	0.33	http://geno	GAIN	No	
WT-G	8	61177726	89924488	rs9969570	rs1050486	28746762	0.67	0.27	0.32	http://geno	GAIN	Yes	
WT-G	8	89945110	90707421	rs963994	rs150615	762312	0.57	0.53	0.3	http://geno	GAIN	No	

WT-G	8	90729636	1,46E+08	rs160449	rs6599566	55534583	0.67	0.28	0.33	http://geno	GAIN	No
WT-G	9	280841	1,4E+08	rs1766453	rs3855758	1,4E+08	0.96	0.02	0.08	http://geno	CNNI	No
WT-G	10	56640222	1,35E+08	rs1050902	rs7895560	78640807	0.72	0.38	0.34	http://geno	GAIN	No
WT-G	12	115596	1,32E+08	rs7974784	rs1114725	1,32E+08	0.67	0.25	0.33	http://geno	GAIN	Yes
WT-G	13	18821153	1,14E+08	rs9554050	rs7327124	95250104	0.67	0.31	0.34	http://geno	GAIN	Yes
WT-G	14	37905490	40974852	rs1168515	rs1013108	3069363	0.85	-0.02	0.08	http://geno	CNNI	No
WT-G	17	22211	78634366	rs2870200	rs6502043	78612155	0.67	0.24	0.34	http://geno	GAIN	Yes
WT-G	20	11799	62371161	rs1418258	rs2427638	62359363	0.67	0.27	0.34	http://geno	GAIN	No
WT-G	23	2753627	1,55E+08	rs5982588	rs557132	1,52E+08	0.96	-0.2	0.28	http://geno	LOSS	Yes
WT-J	12	120500	1,32E+08	rs2291928	rs7975069	1,32E+08	0.58	0.11	0.33	http://geno	GAIN	No
WT-J	13	18110262	1,14E+08	rs1114766	rs7999630	95972323	0.58	0.13	0.32	http://geno	GAIN	No
WT-J	16	32530051	88668856	rs1948865	rs1292593	56138806	0.62	-0.12	0.33	http://geno	LOSS	No
WT-J	20	11799	62371161	rs1418258	rs2427638	62359363	0.58	0.12	0.35	http://geno	GAIN	No
WT-L	1	1,44E+08	2,47E+08	rs1079764	rs9727917	1,03E+08	0.62	0.18	0.32	http://geno	GAIN	Yes
WT-L	3	70973	1,99E+08	rs1400176	rs1015490	1,99E+08	0.64	0.17	0.34	http://geno	GAIN	Yes
WT-L	6	150800	14318442	rs1418707	rs1537147	14167643	0.61	0.17	0.33	http://geno	GAIN	No
WT-L	6	14323808	15584027	rs6911584	rs2064100	1260220	0.83	-0.05	0.34	http://geno	CNNI	No
WT-L	6	15600681	30053599	rs2237122	rs2246199	14452919	0.61	0.16	0.3	http://geno	GAIN	No
WT-L	6	47819559	1,71E+08	rs1890061	rs1080687	1,05E+08	0.62	0.17	0.32	http://geno	GAIN	Yes
WT-L	10	149076	38541660	rs4881551	rs1780138	38392584	0.76	-0.25	0.34	http://geno	LOSS	Yes
WT-L	12	36407203	1,32E+08	rs1663281	rs7975069	95881667	0.62	0.18	0.32	http://geno	GAIN	No
WT-L	15	18421386	1E+08	rs6599770	rs7181527	81794198	0.62	0.18	0.33	http://geno	GAIN	No
WT-L	16	45096893	88668856	rs9935841	rs1292593	43571964	0.76	-0.22	0.32	http://geno	LOSS	No
WT-L	18	111949	76116152	rs2847087	rs1296063	76004204	0.63	0.2	0.34	http://geno	GAIN	No
WT-M	5	1,78E+08	1,79E+08	rs1445844	rs1760715	179063	0.62	0.2	0.78	http://geno	GAIN	No
WT-M	11	31177288	32083514	rs158136	rs6711	906227	0.93	-0.45	0.45	http://geno	LOSS	No
WT-M	11	32021832	32423225	rs224619	rs3858451	401394		-2.22		http://geno	LOSS	No
WT-M	11	32454931	35356213	rs2067666	rs2065030	2901283	0.93	-0.37	0.3	http://geno	LOSS	No
WT-N	22	15464609	17372121	rs2070501	rs5993462	1907513	0.57	0.08	0.34	http://geno	GAIN	
WT-N	22	17405381	49531259	rs6623	rs7284680	32125879	0.64	-0.14	0.34	http://geno	LOSS	No
WT-O	7	149081	56204774	rs7806592	rs816396	56055694	0.98	-0.39	0.22	http://geno	LOSS	No
WT-O	7	61100583	64546648	rs1113561	rs4717259	3446066	0.64	0.25	0.33	http://geno	GAIN	No
WT-O	7	64937858	66331505	rs3573512	rs3436657	1393648	0.97	0.16	0.16	http://geno	GAIN	No
WT-O	7	66471076	1,59E+08	rs2421292	rs1124425	92341171	0.63	0.2	0.35	http://geno	GAIN	Yes
WT-O	11	213272	44934752	rs3782115	rs4755921	44721481	0.98		0	0.12	http://geno	CNNI	No
WT-P	4	1,04E+08	1,06E+08	rs223502	rs2726513	2577002	0.82	-0.4	0.47	http://geno	LOSS	No
WT-P	5	98541724	1E+08	rs1005652	rs1006508	1848246	0.82	-0.46	0.41	http://geno	LOSS	Yes
WT-P	11	213272	47121682	rs3782115	rs7121418	46908411	0.98	0.02	0.03	http://geno	CNNI	No
WT-P	11	47443461	49685221	rs1317149	rs7934062	2241761	0.96	-0.09	0.1	http://geno	LOSS	No
WT-P	22	44635144	47046698	rs2097429	rs133590	2411555	0.98	-0.34	0.2	http://geno	LOSS	No
WT-Q	2	2,02E+08	2,12E+08	rs2676325	rs714393	10195493	0.71	-0.2	0.28	http://geno	LOSS	Yes
WT-Q	2	2,14E+08	2,4E+08	rs2099799	rs3791500	25958270	0.68	-0.17	0.36	http://geno	LOSS	No
WT-Q	7	162448	63066168	rs3924854	rs7808552	62903721	0.57	-0.08	0.33	http://geno	LOSS	No
WT-Q	10	149076	37560631	rs4881551	rs1926127	37411556	0.68	-0.17	0.31	http://geno	LOSS	No
WT-Q	11	193788	36784445	rs2280543	rs1518754	36590657	0.76		0	0.36	http://geno	CNNI	Yes
WT-Q	16	45627130	88668856	rs1164056	rs1292593	43041726	0.68	-0.16	0.35	http://geno	LOSS	Yes
WT-S	1	1084601	99552872	rs4970362	rs712878	98468271	0.89	-0.33	0.34	http://geno	LOSS	Yes
WT-S	1	1,01E+08	1,04E+08	rs7516666	rs6664203	3833413	0.89	-0.4	0.62	http://geno	LOSS	Yes
WT-S	4	63508	1,91E+08	rs4690284	rs1597620	1,91E+08	0.89	-0.32	0.36	http://geno	LOSS	Yes
WT-S	9	195964	1,4E+08	rs478882	rs3750508	1,4E+08	0.88	-0.32	0.35	http://geno	LOSS	Yes
WT-S	11	189256	1,34E+08	rs3741411	rs1182189	1,34E+08	0.88	-0.32	0.36	http://geno	LOSS	Yes
WT-S	12	1,13E+08	1,13E+08	rs1035775	rs726424	247534	0.65	0.23	0.43	http://geno	GAIN	No
WT-S	13	79702503	79967277	rs348008	rs6563169	264775	0.67	0.32	0.65	http://geno	GAIN	No
WT-S	14	21678306	23749717	rs6572287	rs2295322	2071412	0.64	0.16	0.27	http://geno	GAIN	No
WT-S	14	23963051	1,06E+08	rs1004664	rs2003168	82164348	0.89	-0.32	0.33	http://geno	LOSS	Yes

Full Materials and Methods

Materials

The study was approved by the Lund Ethics Committee and by the review boards of the collaborating institutes. Informed consent had been obtained prior to investigation of tissue samples. Short term cultures established from fibroblasts and primary tumors were sub-cultured no more than five times before analysis. The cell lines from individuals with mosaic variegated aneuploidy syndrome were obtained with informed consent and multicenter research ethics approval (MREC05/02/17). MVA12 has biallelic *BUB1B* mutations 2211-2212insGTTA _S738fsX753 and c.2441G>A_p.R814H and has been previously reported in Hanks *et al.* (1) where it was cited as Family 2. MVA41 has mutations c.2144-2A>G and c.464A>G_ p.Y155C. No *BUB1B* mutation was identified in MVA28 despite full screening of the gene. The colorectal cancer cell lines SW480, LoVo, and DLD1 were obtained from the American Type Culture Collection and WiT49 was kindly donated by Dr. Herman Yeger at the Laboratory of Medicine and Pathobiology, University of Toronto, Canada. HEK293D cells were obtained from The Banca Cellule e Colture in GMP, Genova, Italy. Both WiT49 cells and HEK293 contained multipolar cell divisions, invariably coordinated by multiple centrosomes (2). The construct and transfection procedure used to create HEK293D *H2B-GFP* cells have been previously described (3). In brief, full length *H2B* was amplified and cloned between into the pEGFP-N1 vector (Clontech, Mountain View, CA), with the 5' end in frame with the cDNA coding for enhanced green fluorescence protein. For transfection, the Lipofect-AMINE 2000 reagent was used (Invitrogen Life Technologies, Carlsbad, CA) according to instructions provided by the manufacturer for HEK293 cells. After five days of growth in medium containing 1 mg/ml Geneticin, 75% of nuclei were GFP-positive. Tissue sections used for mapping of trisomic clones were selected from two pediatric Wilms tumours after histopathological review.

Fluorescence in situ hybridisation (FISH) and immunofluorescence on cultured cells

Cell culture, fixation, FISH, and immunofluorescence were performed as described previously (3). Chromosome segregation was scored by FISH in ana-telophase cells using centromeric probes (Abbott Molecular, Abbott Park, IL), supplemented with single-copy probes for chromosome arms 13q and 21q (fibroblasts only). This supplementary probe set was included to exclude significant intra-chromosomal variation in the rate of missegregation. In each case, 810-3112 chromosome segregation events were scored. Missegregation rates was calculated as the number of missegregation events observed in a cell population, including all probes used, divided by the total number of chromosome segregations scored in the cell population by these probes. In HEK293D cells, tri-colour FISH was performed after GFP-fluorescence had been completely bleached off through heat denaturation, allowing also the use of probes with green spectral emission (FITC). Beta-tubulin was detected by the monoclonal antibody TUB2.1 O95K4841 (Sigma-Aldrich, St. Louis, MO), MAD2L1 by ab24588 (Abcam, Cambridge, UK), and Aurora kinase A by A300-071A (Bethyl Laboratories Inc., Montgomery, TX).

Time lapse microscopy

For time lapse holographic microscopy, WiT49 cells were seeded in an Ibidi μ-slide I (Integrated BioDiagnostics, Munich, Germany) coated with IbiTreat. The slide was kept on an Ibidi HT-50 heating stage (Integrated BioDiagnostics) set to 37°C with medium manually changed every 2-3 days. Holograms were captured using HoloMonitor M2 (Phase Holographic Imaging AB, Lund, Sweden) and reconstructed into three-dimensional images using the HStudio 1.8 software with readjustment of focal depth allowing time-lapse sequences without drifting out of focus for more than eight days. Only cells entering multipolar metaphase followed by tripolar anaphase, were included in the time-lapse studies. Images were acquired at 2-5 minute intervals. For time lapse phase-contrast/fluorescence microscopy, HEK293D cells were seeded in an Ibidi μ-slide I and kept at 37°C as described above. Because all

imaging sessions were <72 h, medium was not changed during the imaging process.

Modelling frequencies of trisomies and tetrasomies

Based on previous studies (3), calculations were made with the assumption of a random distribution of chromosomes along the metaphase plate. Sex chromosomes were excluded from all calculations and comparisons with cytogenetic data. For cell populations with trisomies generated concurrently by tripolar chromosome segregation followed by cytokinesis along one cleavage furrow, the relative frequency of tetrasomic cases was calculated according to the series 1-(44-2)/(44-1)x(44-4)/(44-2)x(44-6)/(44-3)…x(44-2(N-1))/(44-(N-1)), where N is the number of extra chromosomes in the hyperdiploid daughter cell. For cell populations undergoing sequential accumulation of extra chromosomes through non-disjunction, the relative frequency of cases with at least one tetrasomy was calculated according to the series 1-(44-2)/(44+1)x(44-4)/(44+2)x(44-6)/(44+3)……x(46-2N)/(43+N), where N is the number of extra chromosomes in the hyperdiploid cell. Cytogenetic data were retrieved from the Mitelman Database of Chromosome Aberrations in Cancer (http://cgap.nci.nih.gov/Chromosomes/Mitelman; last access Feb. 1, 2010). Only karyotypes with chromosome numbers 46-69 with at least two whole chromosome gains, without the annotations "inc" (incomplete karyotype) and "?" (questionable identification of a chromosome or chromosome structure) were included. Chromosome gains were always scored in relation to the diploid level. Related clones were merged (18 cases). Unrelated clones, found in one case, were treated as separate cases. These selection criteria allowed the inclusion of 152/422 reported cases.

SNP-based array comparative genomic hybridization

For concurrent high-resolution detection of genomic imbalances, 300 ng of DNA extracted using standard methods (DNeasy Blood & Tissue Kit, Qiagen, Valencia, CA) was hybridized to Illumina HumanCNV370-Duo/Quad Genotyping BeadChips (Illumina Inc., San Diego, CA) according to the

manufacturer's specifications. Allele specific fluorescent signals were first normalized using a proprietary algorithm in the Illumina BeadStudio software (Illumina Inc). Normalized allelic intensity values were thereafter exported and subjected to an additional normalization step using the tQN-software (4). By applying a threshold-modified quantile normalization algorithm, this normalization method corrects for the dye-dependent asymmetry between the two different fluorescent channels that has been observed in Illumina Infinium data. The tQN software was also used to estimate B-allele frequencies (BAF) for each SNP based on a set of reference genotype clusters. For identification of imbalances, the BAF segmentation software was used, in which BAF-values are transformed into mirrored BAF (mBAF) values followed by removal of non-informative homozygous SNPs by a fixed mBAF threshold (5). BAF segmentation also applies a segmentation algorithm on the mBAF data to define regions of allelic imbalance. For each resulting segment, a copy number estimate is also given as the median log2 ratio of all SNPs present within the defined segment. Segments with mBAF values >0.55 were classified as being in allelic imbalance. Segments with log2 ratio >0.073 were classified as genomic gains, those with log2 ratios <0.080 as genomic losses, and those with log2 ratios between these boundaries as copy number neutral genomic imbalances. Copy number imbalances that were not associated with allelic imbalances (*e.g.* 4 copies at a 2:2 ratio) were identified by visual inspection of log2 ratio plots. Segments were fused if the interspersed genomic distance was <1 Mb and the difference in mBAF values between the segments was <0.1. Constitutional copy number variants were excluded from the final data by comparison to the Database of Genomic Variants (http://projects.tcag.ca/variation/; last access Sept. 1 2009). Segmented SNP-array data, without constitutional variants and other patient-specific genotype information, are included in Supporting Data File S1. mBAF values were used to estimate the proportion of sampled DNA containing the respective genomic imbalances, calculated according to equations detailed by described by Staaf *et al.* (5). This approach has previously been shown by FISH-validation to accurately predict the proportion of cells carrying genomic imbalances in tumors with known ploidy levels. The chosen mBAF threshold of 0.56

for calling allelic imbalances allowed detection of hemizygous losses present in clones exceeding 20% of and single copy gains (*e.g.* trisomies) in clones exceeding 25% of sampled cells. Based on previous comparisons between FISH data and mBAF values (5), a difference in mBAF exceeding 0.01 was used to build confidence intervals for clone size (proportion of tumor cells). Proportions with non-overlapping confidence intervals were scored as significantly different from each other.

FISH on tissue sections

Tissue sections of 4 μm were prepared on positively charged microscopy slides according to standard procedures and deparaffinized in xylene for 3x5 minutes, followed by rehydration in a graded ethanol series, and washing in phosphate-buffered saline. Target DNA accessibility was increased by treatment for 15-25 min in antigen retrieval buffer (DAKO, Glostrup, Denmark) at 125°C. This was followed by 20 mg/ml pepsin treatment for 5 min at 37°C in 0.01 M HCl, washing in saline, and dehydration prior to co-denaturation of probe and target DNA at 84°C for 10 min. Areas containing at least 30 nuclei were evaluated for copy number of a selected chromosome by comparing the total number of centromere probe signals for this chromosome to a chromosome known from previous single nucleotide polymorphism (SNP)-based array comparative genomic hybridization to be disomic in the tumour. Reference values for disomy (expected ratio 2:2) were calculated as 1.0 +/- 2x(coefficient of variance) in cells located in normal kidney parenchyma or the kidney capsule, typically resulting in reference intervals of 0.85-1.15, while reference numbers for trisomies (expected ratio 3:2) were calculated as 1.5 +/- 2x(coefficient of variance) typically resulting in reference intervals of 1.25-1.75.

References

1.   Hanks S, et al. (2004) Constitutional aneuploidy and cancer predisposition caused by biallelic mutations in BUB1B. *Nat Genet* 36:1159-1161. 1. Hanks S, et al. (2004) Constitutional aneuploidy and cancer predisposition caused by biallelic mutations in BUB1B. *Nat Genet* 36:1159-1161.

2.   Stewénius Y, et al. (2007) Defective chromosome segregation and telomere dysfunction in aggressive Wilms tumours *Clin Cancer Res* 13:6593-6602.

3.   Gisselsson D, et al. (2008) When the genome plays dice: circumvention of the spindle assembly checkpoint and near-random chromosome segregation in multipolar cancer cell mitoses. *PLoS ONE* 3:e1871.

4.   Staaf J, et al. (2008) Normalization of Illumina Infinium whole-genome SNP data improves copy number estimates and allelic intensity ratios. *BMC Bioinformatics* 9:409.

5.   Staaf J, et al. (2008) Segmentation-based detection of allelic imbalance and loss-of-heterozygosity in cancer cells using whole genome SNP arrays. *Genome Biol* 9:R136.